

Eur. Phys. J. A (2016) **52**: 231

DOI 10.1140/epja/i2016-16231-x

## Supporting the search for the CEP location with nonlocal PNJL models constrained by lattice QCD

Gustavo A. Contrera, A. Gabriela Grunfeld and David Blaschke



# Supporting the search for the CEP location with nonlocal PNJL models constrained by lattice QCD<sup>\*</sup>

Gustavo A. Contrera<sup>1,2,3,a</sup>, A. Gabriela Grunfeld<sup>3,4</sup>, and David Blaschke<sup>5,6,7</sup>

<sup>1</sup> IFLP, UNLP, CONICET, Facultad de Ciencias Exactas, calle 49 y 115, La Plata, Argentina

<sup>2</sup> Gravitation, Astrophysics and Cosmology Group, FCAyG, UNLP, La Plata, Argentina

<sup>3</sup> CONICET, Rivadavia 1917, 1033 Buenos Aires, Argentina

<sup>4</sup> Departamento de Física, Comisión Nacional de Energía Atómica, (1429) Buenos Aires, Argentina

<sup>5</sup> Institute for Theoretical Physics, University of Wrocław, 50-204 Wrocław, Poland

<sup>6</sup> Joint Institute for Nuclear Research, 141980 Dubna, Moscow Region, Russia

<sup>7</sup> National Research Nuclear University (MEPhI), 115409 Moscow, Russia

Received: 27 May 2016 / Revised: 21 July 2016

Published online: 19 August 2016 – © Società Italiana di Fisica / Springer-Verlag 2016

Communicated by T. Biro

**Abstract.** We investigate the possible location of the critical endpoint in the QCD phase diagram based on nonlocal covariant PNJL models including a vector interaction channel. The form factors of the covariant interaction are constrained by lattice QCD data for the quark propagator. The comparison of our results for the pressure including the pion contribution and the scaled pressure shift  $\Delta P/T^4$  vs.  $T/T_c$  with lattice QCD results shows a better agreement when Lorentzian form factors for the nonlocal interactions and the wave function renormalization are considered. The strength of the vector coupling is used as a free parameter which influences results at finite baryochemical potential. It is used to adjust the slope of the pseudocritical temperature of the chiral phase transition at low baryochemical potential and the scaled pressure shift accessible in lattice QCD simulations. Our study, albeit presently performed at the mean-field level, supports the very existence of a critical point and favors its location within a region that is accessible in experiments at the NICA accelerator complex.

The search for the location of the critical endpoint (CEP) of first-order phase transitions in the QCD phase diagram is one of the objectives for beam energy scan (BES) programs in relativistic heavy-ion collision experiments at RHIC and SPS as well as in future ones at NICA and FAIR, which try to identify the parameters of its position ( $T_{\text{CEP}}, \mu_{\text{CEP}}$ ). From a theoretical point of view, the situation is very blurry since the predictions for this position form merely a skymap in the  $T$ - $\mu$  plane [1].

Lattice QCD results at zero and small chemical potential  $\mu$  show that the chiral and deconfinement transitions are crossover with a pseudocritical temperature of  $T_c(0) = 154 \pm 9$  MeV [2].

However, at finite density lattice QCD suffers from the sign problem and only extrapolation or approximate techniques are available that work at finite quark densities. Therefore, nonperturbative methods and effective models are inevitable tools in this region. Up to now, such effective

low-energy QCD approaches are not yet sufficiently developed to provide a unified approach to quark-hadron matter where hadrons appear as strongly correlated (bound) quark states that eventually dissolve into their quark (and gluon) constituents in the transition from the hadronic phase with confined quarks to the quark gluon plasma. Since this transition shall be triggered by chiral symmetry restoration (by lowering the thresholds for hadron dissociation determined by in-medium quark masses), we expect that a first step towards a theoretical approach to the QCD phase diagram is the determination of order parameters characterizing the QCD phases in a mean-field approximation for chiral quark models of different degree of sophistication. As a consequence there appeared a variety of possibilities for the structure of the QCD phase diagram and the position of the CEP in the literature. Let us mention few of them:

- no CEP at all [3], with crossover transition in the whole phase diagram;
- no CEP, but a Lifshitz point [4];
- one CEP, but with largely differing predictions of its position [1];

<sup>\*</sup> Contribution to the Topical Issue “Exploring strongly interacting matter at high densities - NICA White Paper” edited by David Blaschke *et al.*

<sup>a</sup> e-mail: [contrera@fisica.unlp.edu.ar](mailto:contrera@fisica.unlp.edu.ar)

- second CEP [5–7];
- CEP and triple point, possibly coincident, considering another phase (*i.e.* color superconducting [8] or quarkyonic [9] matter) at low temperatures and high densities.

This situation is far from being satisfactory in view of the upcoming experimental programmes. An exhaustive analysis should be performed to predict a CEP region as narrow as possible, considering only those effective models that best reproduce recent lattice QCD results, on the one hand, and that obey constraints from heavy-ion collision experiments and compact star observations where available.

In the present contribution, we discuss the existence and location of a CEP within the class of nonlocal chiral quark models coupled to the Polyakov loop (PL) potential, with vector channel interactions, on the self-consistent mean-field level, contrasting our results with those of the widely used local PNJL models that appear as limiting case of the present approach.

The Lagrangian of these models is given by

$$\mathcal{L} = \bar{q}(i\not{D} - m_0)q + \mathcal{L}_{\text{int}} + \mathcal{U}(\Phi), \quad (1)$$

where  $q$  is the  $N_f = 2$  fermion doublet  $q \equiv (u, d)^T$ , and  $m_0$  is the current quark mass (we consider isospin symmetry, that is  $m_0 = m_u = m_d$ ). The covariant derivative is defined as  $D_\mu \equiv \partial_\mu - iA_\mu$ , where  $A_\mu$  are color gauge fields.

The nonlocal interaction channels are given in the current-current coupling form by

$$\begin{aligned} \mathcal{L}_{\text{int}} = & -\frac{G_S}{2} [j_a(x)j_a(x) - j_P(x)j_P(x)] \\ & -\frac{G_V}{2} j_V(x)j_V(x), \end{aligned} \quad (2)$$

where the nonlocal generalizations of the currents are

$$\begin{aligned} j_a(x) &= \int d^4z g(z) \bar{q}\left(x + \frac{z}{2}\right) \Gamma_a q\left(x - \frac{z}{2}\right), \\ j_P(x) &= \int d^4z f(z) \bar{q}\left(x + \frac{z}{2}\right) \frac{i \overleftrightarrow{\not{D}}}{2\kappa_p} q\left(x - \frac{z}{2}\right), \\ j_V(x) &= \int d^4z g(z) \bar{q}\left(x + \frac{z}{2}\right) \gamma^0 q\left(x - \frac{z}{2}\right), \end{aligned} \quad (3)$$

with  $\Gamma_a = (\Gamma_S, \Gamma_P) = (\mathbb{1}, i\gamma_5\boldsymbol{\tau})$  for scalar and pseudoscalar currents respectively, and  $u(x') \overleftrightarrow{\not{D}} v(x) = u(x')\partial_x v(x) - \partial_{x'} u(x')v(x)$ . The functions  $g(z)$  and  $f(z)$  in eq. (3) are nonlocal covariant form factors characterizing the corresponding interactions. The scalar-isoscalar component of the  $j_a(x)$  current will generate the momentum-dependent quark mass in the quark propagator, while the ‘‘momentum’’ current,  $j_P(x)$ , will be responsible for a momentum-dependent wave function renormalization (WFR) of this propagator. Note that the relative strength between both interaction terms is controlled by the mass parameter  $\kappa_p$  introduced in eq. (3). Finally,  $j_V(x)$  represents the vector channel interaction current, whose coupling constant  $G_V$  is usually taken as a free parameter.

In what follows it is convenient to Fourier transform into momentum space. Since we are interested in studying the characteristics of the chiral phase transition we have to extend the effective action to finite temperature  $T$  and chemical potential  $\mu$ . In the present work this is done by using the Matsubara imaginary time formalism. Concerning the gluon degrees of freedom we employ the PL extension of nonlocal chiral quark models according to previous works [10–14], *i.e.* assuming that the quarks move in a background color gauge field  $\phi = iA_0 = ig\delta_{\mu 0} G_a^\mu \lambda^a/2$ , where  $G_a^\mu$  are the SU(3) color gauge fields and  $\lambda^a$  are the Gell-Mann matrices. Then the traced PL  $\Phi$ , which is taken as order parameter of confinement, is given by  $\Phi = \frac{1}{3} \text{Tr} \exp(i\phi/T)$ . Then, working in the so-called Polyakov gauge, in which the matrix  $\phi$  is given by a diagonal representation  $\phi = \phi_3 \lambda_3 + \phi_8 \lambda_8$ . At vanishing chemical potential, owing to the charge conjugation properties of the QCD Lagrangian, the traced PL is expected to be a real quantity. Since  $\phi_3$  and  $\phi_8$  have to be real-valued [15], this condition implies  $\phi_8 = 0$ . In general, this need not be the case at finite  $\mu$  [16,17]. As, *e.g.*, in refs. [11,15,18–20] we will assume that the potential  $\mathcal{U}$  is such that the condition  $\phi_8 = 0$  is well satisfied for the range of values of  $\mu$  and  $T$  investigated here. The mean-field-traced PL is then given by

$$\Phi = \frac{1}{3} [1 + 2 \cos(\phi_3/T)]. \quad (4)$$

In the present work we have chosen a  $\mu$ -dependent logarithmic effective potential described in [21],

$$\begin{aligned} \mathcal{U}(\Phi, T, \mu) = & (a_0 T^4 + a_1 \mu^4 + a_2 T^2 \mu^2) \Phi^2 \\ & + a_3 T_0^4 \ln(1 - 6\Phi^2 + 8\Phi^3 - 3\Phi^4), \end{aligned} \quad (5)$$

where there parameters are  $a_0 = -1.85$ ,  $a_1 = -1.44 \times 10^{-3}$ ,  $a_2 = -0.08$ ,  $a_3 = -0.40$ . For the  $T_0$  parameter we use the value corresponding to two flavors  $T_0 = 208$  MeV, as has been suggested in ref. [22] and already employed in nonlocal PNJL models in [12,23].

Finally, in order to fully specify the nonlocal model under consideration we set the model parameters as well as the form factors  $g(q)$  and  $f(q)$  following refs. [11,24] and [25], *i.e.* considering two different types of functional dependencies for these form factors: exponential forms

$$\text{(Set A)} \quad \begin{cases} g(p) = \exp(-p^2/\Lambda_0^2) \\ f(p) = 0, \end{cases} \quad (6)$$

$$\text{(Set B)} \quad \begin{cases} g(p) = \exp(-p^2/\Lambda_0^2) \\ f(p) = \exp(-p^2/\Lambda_1^2), \end{cases} \quad (7)$$

and Lorentzians with WFR

$$\text{(Set C)} \quad \begin{cases} g(p) = \frac{1 + \alpha_z}{1 + \alpha_z f_z(p)} \frac{\alpha_m f_m(p) - m \alpha_z f_z(p)}{\alpha_m - m \alpha_z} \\ f(p) = \frac{1 + \alpha_z}{1 + \alpha_z f_z(p)} f_z(p), \end{cases} \quad (8)$$

where

$$\begin{aligned} f_m(p) &= \left[1 + (p^2/A_0^2)^{3/2}\right]^{-1}, \\ f_z(p) &= \left[1 + (p^2/A_1^2)\right]^{-5/2}, \end{aligned} \quad (9)$$

and  $\alpha_m = 309 \text{ MeV}$ ,  $\alpha_z = -0.3$ . Further details on the parameters can be found in ref. [25] and references quoted therein.

Within this framework the thermodynamic potential in the mean-field approximation (MFA) reads

$$\begin{aligned} \Omega^{\text{MFA}} &= -4T \sum_c \sum_n \int \frac{d^3\mathbf{p}}{(2\pi)^3} \ln \left[ \frac{(\tilde{\rho}_{n,\mathbf{p}}^c)^2 + M^2(\rho_{n,\mathbf{p}}^c)}{Z^2(\rho_{n,\mathbf{p}}^c)} \right] \\ &+ \frac{\sigma_1^2 + \kappa_p^2 \sigma_2^2}{2G_S} - \frac{\omega^2}{2G_V} + \mathcal{U}(\Phi, T), \end{aligned} \quad (10)$$

where  $M(p)$  and  $Z(p)$  are given by

$$\begin{aligned} M(p) &= Z(p) [m + \sigma_1 g(p)], \\ Z(p) &= [1 - \sigma_2 f(p)]^{-1}. \end{aligned} \quad (11)$$

In addition, we have defined [26]

$$(\rho_{n,\mathbf{p}}^c)^2 = [(2n+1)\pi T - i\mu + \phi_c]^2 + \mathbf{p}^2, \quad (12)$$

where the quantities  $\phi_c$  are given by the relation  $\phi_c = \text{diag}(\phi_r, \phi_g, \phi_b)$ . Namely,  $\phi_c = c\phi_3$  with  $c = 1, -1, 0$  for  $r, g, b$ , respectively.

In the case of  $(\tilde{\rho}_{n,\mathbf{p}}^c)$  we have used the same definition as in eq.(12) but shifting the chemical potential according to [25]

$$\tilde{\mu} = \mu - \omega g(p) Z(p). \quad (13)$$

We also want to include in our analysis the results arising from a local PNJL model based on [27] with two flavors instead of three. Moreover, we consider that the chemical potential is shifted by

$$\tilde{\mu} = \mu - \omega. \quad (14)$$

$\Omega^{\text{MFA}}$  turns out to be divergent and, thus, needs to be regularized. For this purpose we use the same prescription as in refs. [28,11]. The mean-field values  $\sigma_{1,2}$ ,  $\omega$  and  $\phi_3$  at a given temperature or chemical potential, are obtained from a set of four coupled ‘‘gap’’ equations which come from the minimization of the regularized thermodynamic potential, that is

$$\frac{\partial \Omega_{\text{reg}}^{\text{MFA}}}{\partial \sigma_1} = \frac{\partial \Omega_{\text{reg}}^{\text{MFA}}}{\partial \sigma_2} = \frac{\partial \Omega_{\text{reg}}^{\text{MFA}}}{\partial \omega} = \frac{\partial \Omega_{\text{reg}}^{\text{MFA}}}{\partial \phi_3} = 0. \quad (15)$$

As a starting point, we consider the local NJL, using in this case the parameters as in [20]. This resembles the local limit of the present model and results can be compared, *e.g.*, with refs. [3] and [29]. As in our previous work [25], the model inputs have been constrained with results from lattice QCD studies. In particular, the form factors of the nonlocal interaction can be chosen such as to reproduce

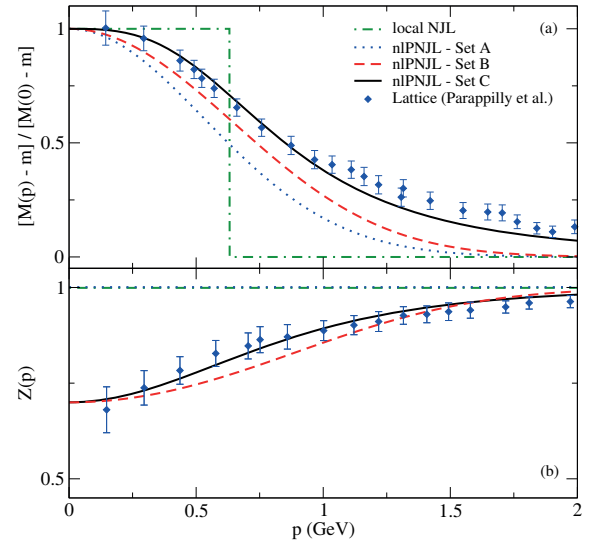


**Fig. 1.** Normalized dynamical masses for the different form factors under study and wave function renormalization for Set B and Set C, fitted to lattice QCD data [30]. (Adapted from ref. [24]).

the dynamical mass function  $M(p)$  and the WFR function  $Z(p)$  of the quark propagator in the vacuum [30]. In fig. 1 we show the shapes of normalized dynamical masses and WFR for the models under discussion here, *i.e.*, the nonlocal models of Set A (rank-one), Set B and Set C (rank-two) as well as the local limit. From this figure we see that Set C fits best the normalized dynamical mass.

Now we are in the position to discuss the results for the thermodynamics of the nonlocal PNJL models, starting from the pressure  $P(\mu, T) = -\Omega_{\text{reg}}^{\text{MFA}}$ . In the upper panel of fig. 2, we compare the pressure shift  $\Delta P = P(\mu, T) - P(0, T)$  scaled with  $T^4$  as a function of  $T/T_c$  for all sets of parametrizations shown in fig. 1 to lattice results from [31,32]. It is obvious that the best obtained fit corresponds to Set C, supporting the robustness of rank-2 Lorentzian parametrization. In the lower panel of fig. 2, we show a comparison between Set C and lattice results [31], for  $G_V = 0.0$  (*i.e.* without vector interactions).

In fig. 3, we show a comparison of the pressure normalized to the Stefan-Boltzmann limit ( $P_{\text{SB}}$ ) to lattice QCD results from [33]. In this figure it can be seen that the pion pressure dominates the pressure dependence for  $T < T_c$  and quickly vanishes for  $T > T_c$  as a result of the Mott dissociation of the pion.

From the above results, Set C appears to be the appropriate choice to best fit lattice QCD results.

As mentioned above, the vector coupling  $G_V$  is considered a free parameter. In fig. 4 we show again  $\Delta P/T^4$  *vs.*  $T/T_c$  as in fig. 2, but now considering different vector coupling parameters  $\eta_V = G_V/G_S$  just for Set C and  $\mu = T_c$ . The best agreement with lattice QCD data is obtained for  $\eta_V = 0$ , *i.e.* for the deactivated vector channel. The consequences will be discussed below.

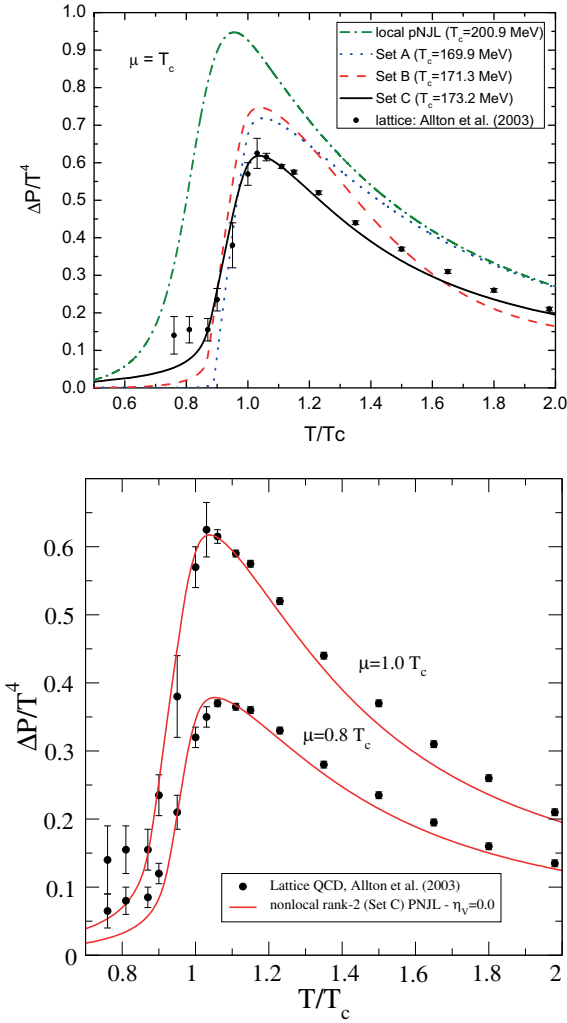


**Fig. 2.** The scaled pressure shift  $\Delta P/T^4$  as a function of the scaled temperature  $T/T_c$ , for  $G_V = 0.0$ . Upper panel: Comparison of the lattice QCD data [31] with results of local and non-local pNJL models. Lower panel: Comparison of Set C results with lattice QCD [31] for two chemical potentials  $\mu = 1.0 T_c$  and  $\mu = 0.8 T_c$ .

In MFA the vector coupling channel has a direct influence on the  $\mu$  dependence of the pseudocritical temperature  $T_c(\mu)$  in the QCD phase diagram. In lattice QCD this dependence has been analyzed by Taylor expansion techniques [34] as

$$T_c(\mu)/T_c(0) = 1 - \kappa(\mu/T)^2 + \mathcal{O}[(\mu/T)^4], \quad (16)$$

with  $\kappa = 0.059(2)(4)$  being the curvature. We will refer to this situation as LR I (lattice results I). In the same way, the vector coupling channel can be tuned to reproduce the curvature given by recent lattice QCD results based on imaginary chemical potential technique which gives  $\kappa = 0.1341 \pm 0.019$  [35] and  $\kappa = 0.1215 \pm 0.018$  [36], we call it LR II.

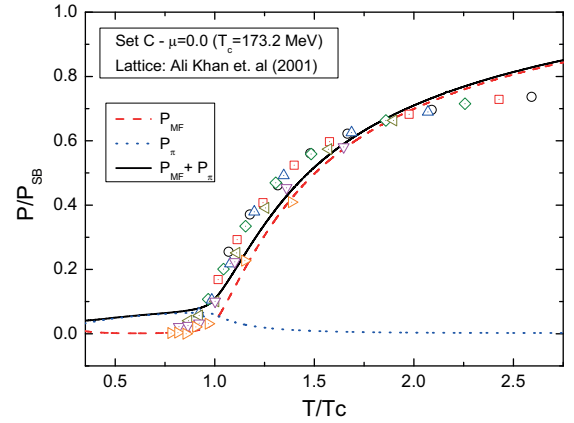


**Fig. 3.** Comparison of the pressure in units of its Stefan-Boltzmann value between Set C (with and without pion pressure) and lattice QCD results [33] as a function of  $T/T_c$ .

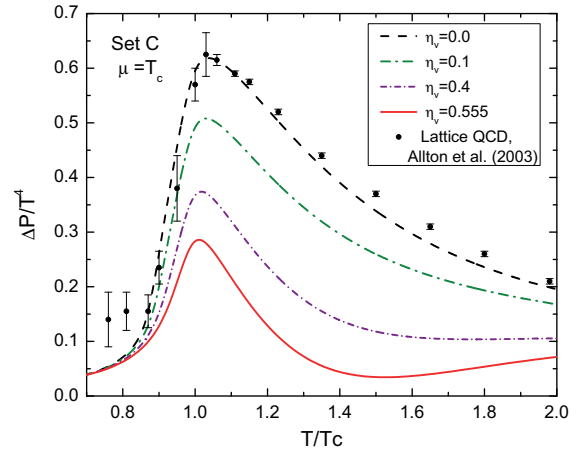


**Fig. 4.** Comparison between Set C results for different values of the vector coupling parameter  $\eta_V$  and lattice QCD data [31].

The curvatures can be determined from the phase diagrams. To do so, we plotted the pseudocritical temperatures of the crossover transitions as a function of  $(\mu/T)^2$  for different values of the vector coupling parameter  $\eta_V$ . Then, the curvatures can be obtained from the slope of the straight lines in the region of low  $(\mu/T)$  values.

An example of this is shown in fig. 5 for Set C (the corresponding plots for the other sets are qualitatively very similar). The fit (16) of the lattice QCD results, LR I, is also shown. The grey zone corresponds to the error in the coefficient  $\kappa$  obtained in [34].

In fig. 6 we compare the lattice QCD results for both, LR I and LR II, with the values for the coefficient  $\kappa$  obtained within all PNJL models under study, considering different values of  $\eta_V$ .

Note that for fitting the lattice QCD value in the local model a larger vector coupling is required than in the nonlocal ones, as is shown in ref. [25]. Also the absolute value of the critical temperature  $T_c(0)$  in the local model is significantly different (larger) than in the nonlocal one.

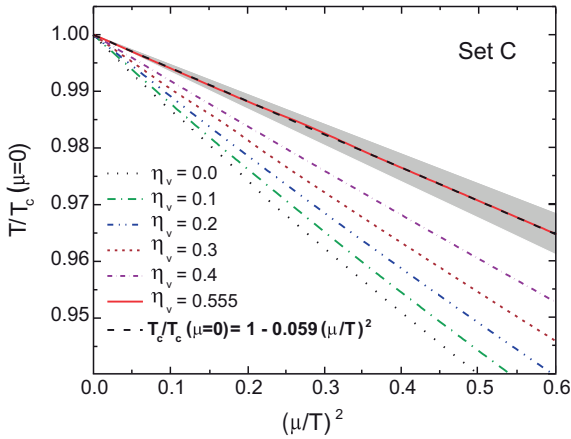


**Fig. 5.** (Color online) Chiral crossover transitions at low values of  $\mu/T$  for different values of the vector coupling ratios  $\eta_V = G_V/G_S$  for Set C. The dashed line corresponds to the lattice QCD prediction of  $\kappa = 0.059(2)(4)$ , LR I [34].

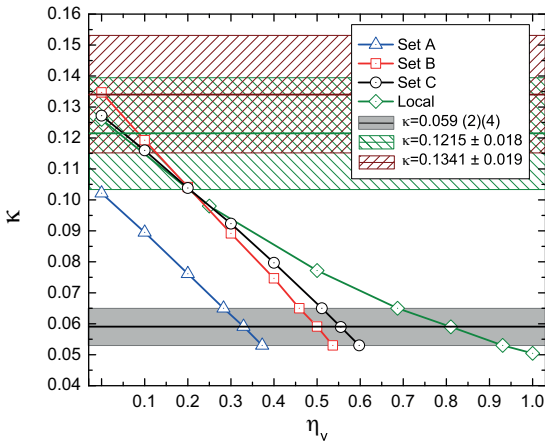


**Fig. 6.** (Color online) Curvature  $\kappa$  of the pseudocritical temperature  $T_c(\mu)$  of the chiral crossover transition at low values of  $\mu/T$ . The black line corresponds to the lattice QCD prediction of  $\kappa = 0.059(2)(4)$  [34], while the brown (green) lines with hatched error regions come from analyses within the imaginary chemical potential method, resulting in  $\kappa = 0.1341 \pm 0.019$  [35] ( $\kappa = 0.1215 \pm 0.018$  [36]).

The phase diagram with (pseudo)critical temperatures  $T_c(\mu)$  and critical points for Set C, *i.e.* the parametrization that best fits lattice QCD results (see figs. 1 to 3) are shown in fig. 7. The finite vector coupling parameter  $\eta_V$  is chosen to reproduce the curvature value for LR I at low  $\mu$ . We found that switching off the vector interaction can reproduce both, the curvature obtained in LR II and the  $\Delta P/T^4$  *vs.*  $T/T_c$  from fig. 2<sup>1</sup>.

Now we also considered the pseudocritical deconfinement lines for  $\Phi = 0.4$ – $0.6$  in fig. 7. To determine them we proceed as follows: we set the fixed value of  $\Phi$  in eq. (4),

<sup>1</sup> Note that in refs. [35,36] the values are quoted in the  $T$ - $\mu_B^2$  plane, while we are addressing the quark chemical potential instead of the baryon one. So the difference in the  $\kappa$  coefficients is a factor 9.

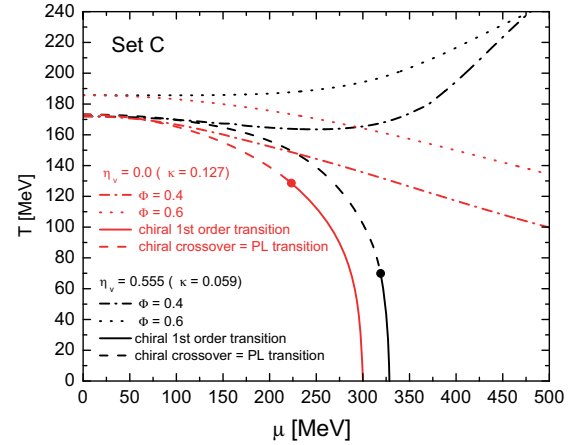


**Fig. 7.** Phase diagrams with (pseudo)critical temperatures  $T_c(\mu)$  and critical endpoints for Set C parametrization of the nonlocal rank-2 PNJL model for the two cases  $\eta_v = 0.0$  and  $\eta_v = 0.555$ . Dashed (full) lines correspond to the chiral crossover (first-order) transitions. The PL transition lines, defined by the peak of the PL susceptibility, coincide with the chiral crossover. The dash-dotted and dotted lines represent the deconfinement transition range, *i.e.*  $\Phi = 0.4$  and  $\Phi = 0.6$ , respectively.

obtaining a relation between  $\phi_3$  and  $T$ . Then we replace this relation in the thermodynamic potential and minimize it respect to the mean fields by solving eqs. (15). Thus, for each value of  $\Phi$  we have the corresponding values of  $\phi_3$  and  $T$  that satisfy eq. (4) and the gaps equations for the desired value of  $\Phi$ . Those are the deconfinement lines at fixed  $\Phi$  shown in fig. 7. However, this tells us only that the PL changes quickly with  $T$ , but not how much confining the model is still at high  $T$ . Since obviously the change occurs at absolute values of  $\Phi \leq 0.4$ , there are still strong color correlations present in the system at high temperatures.

In order to estimate the region in the phase diagram where we expect color correlations as measured by the value of the Polyakov loop to be strong, we choose to show the lines of constant  $\Phi$ . Interestingly, we find that in the presence of a vector mean field the approach to the free quasiparticle case ( $\Phi = 1$ ) is inhibited. It is clear that this is the more so the larger the chemical potential is since the vector mean field is proportional to the baryon density which increases with  $\mu$ .

On the other hand, the PL transition as defined by the peak of the PL thermal susceptibility coincides nicely with that of the crossover chiral transition.

The values for  $T_c(\mu = 0)$  (in MeV) are 169.9, 171.3, 173.2 and 200.9, for Sets A, B, C and local, respectively. These results indicate that the  $T_c(0)$  of nonlocal covariant PNJL models is rather insensitive to the choice of the form factors parametrizing the momentum dependence (running) of the dynamical mass function and the WFR function of the quark propagator as measured on the lattice at zero temperature [30], whereas the position of the CEP and critical chemical potential at  $T = 0$  strongly depends on it.

In view of this finding, the absence of a CEP reported in the local limit [3] as well as the result for Set A without WFR seems to be less realistic (see ref. [25]).

On the other hand, more recent lattice results [35, 36] (LR II) suggest higher values for the  $\kappa$  coefficient, which implies a lower or even vanishing vector coupling parameter  $\eta_V$ , giving better agreement for  $\Delta P/T^4$  vs.  $T/T_c$ .

Considering the different lattice constraints for  $\kappa$  and that the best fitting rank-2 nonlocal PNJL model is the one with Lorentzian form factors (Set C parametrization), the region in the QCD phase diagram where the CEP should be located according to our study, would be determined as  $(T_{\text{CEP}}, \mu_{\text{CEP}}) = (128.6 \text{ MeV}, 223.3 \text{ MeV})$  for  $\eta_V = 0.0$  and  $(T_{\text{CEP}}, \mu_{\text{CEP}}) = (69.9 \text{ MeV}, 319.1 \text{ MeV})$  for  $\eta_V = 0.555$ . This region is highlighted in fig. 7.

With this result of the present study we arrive at our conclusion for the NICA experiments which are devoted to the study of the quark-hadron mixed phase that shall be located at  $T < T_{\text{CEP}}$  and  $\mu > \mu_{\text{CEP}}$ . We shall estimate whether the planned energy ranges of the BM@N experiment ( $E_{\text{lab}} = 2\text{--}4 \text{ A GeV}$ ) and of the MPD experiment ( $\sqrt{s_{NN}} = 4\text{--}11 \text{ GeV}$ ) are suitable for accessing the region of the mixed phase that follows from our study. To this end we use a parametrization for the chemical freeze-out temperature in the QCD phase diagram by Andronic *et al.* [37],

$$T_{\text{freeze}} = T_{\text{lim}} \left( 1 - \frac{1}{0.7 + [\exp(\sqrt{s_{NN}}(\text{GeV})) - 2.9]/1.5} \right), \quad (17)$$

as obtained from statistical model analyses of hadron production in heavy-ion collision experiments, with  $T_{\text{lim}} = 161 \pm 4 \text{ MeV}$ . According to this parametrization and to the LR-I motivated nonlocal PNJL model with vanishing vector coupling, one should expect signals of a first-order phase transition in collisions with  $\sqrt{s_{NN}} \lesssim 6 \text{ GeV}$ , right in the middle of the MPD energy scan. For the LR-II motivated parametrization with  $\eta_V = 0.555$  the CEP is at such a low temperature that only the BM@N experiment has a chance to access the mixed phase, at laboratory energies  $E_{\text{lab}} \lesssim 3 \text{ A GeV}$ , within the range of this fixed target experiment but too low for the collider experiment MPD.

The main conclusion of this study is that for the search of CEP signatures and the investigation of properties of the quark-hadron mixed phase in BES programmes the energy range of the NICA and FAIR facilities shall be particularly promising. We find a certain preference for a CEP position at a critical temperature  $T_{\text{CEP}} \sim 130 \text{ MeV}$ , expected to be crossed in collisions with  $\sqrt{s_{NN}} \sim 6 \text{ GeV}$ , corresponding to  $E_{\text{lab}} \sim 18 \text{ A GeV}$ . This energy could not be reached from above by the present RHIC BES programme of the STAR experiment (lower limit  $\sqrt{s_{NN}} = 7.7 \text{ GeV}$ ) and also not in the NA49 experiment at CERN SPS (lower limit  $E_{\text{lab}} = 20 \text{ A GeV}$ ). Just the ongoing NA61-SHINE experiment has a lower limit of  $E_{\text{lab}} = 13 \text{ A GeV}$  in their energy scan that would allow to cross this suspected critical point (unless it is located at a slightly lower temperature). The old AGS experiment at BNL did not quite reach this energy (maximum energy  $E_{\text{lab}} = 10.74 \text{ A GeV}$ ) and were also not designed for a CEP

search, while the energies at the GSI SIS are probably too low to reach the phase transition border (maximum energy  $E_{\text{lab}} = 2 \text{ A GeV}$ ). The theoretical investigation of the baryon stopping as a probe of the onset of deconfinement in heavy-ion collisions [38] has revealed a characteristic “wiggle” structure in the curvature of the proton rapidity distribution at  $\sqrt{s_{NN}} \sim 6 \text{ GeV}$ , which remains robust also when applying acceptance cuts of the MPD experiment [39] at NICA. The MPD experiment at NICA will be the first dedicated heavy-ion collision experiment of the third generation to fully cover the suspected location of the CEP and thus to enter the mixed phase region via a first-order phase transition. Contrary to studies with the local NJL model which first in [40] and more recently in [3] have shown that a CEP may be absent at all in the phase diagram for finite coupling in the repulsive vector channel, the present work with nonlocal PNJL models constrained by lattice QCD propagator data has shown that the presence of a CEP in the QCD phase diagram is rather robust against even stronger vector channel interactions.

Finally, we would like to mention currently ongoing developments of our approach to the QCD phase diagram and the EoS of matter under extreme conditions:

- Extension of the model to  $2 + 1$  flavours in order to properly compare with modern lattice QCD results [41, 42].
- Investigation of the robustness of the results of the nonlocal PNJL models when modifying the choice of the Polyakov-loop potential taking into account recent developments [43–45].
- Addition of quark pair interaction channels and the possibility of color superconducting quark matter phases [20, 46].
- Going beyond the mean-field approximation within the Beth-Uhlenbeck approach [47], where hadronic correlations of quarks are included with their spectral weight showing both bound and scattering parts, with a characteristic medium dependence that exhibits the Mott transition (dissociation of hadronic bound states into the scattering continuum at finite temperatures and chemical potentials).

A key quantity for such studies is the hadronic phase shifts. First results using a generic ansatz [48] for joining the hadron resonance gas and PNJL approaches are promising [49]. The inclusion of baryonic correlations is possible and has been started at finite temperatures [50] and will be extended to the full phase diagram. As the behavior of the hadronic spectral functions and in particular the location of the Mott transitions in the QCD phase diagram is essentially determined by the dynamical quark mass functions, a key issue for future research is to investigate the back-reaction of hadronic correlations on these order parameters. We expect that, by following the Beth-Uhlenbeck approach, one will have a methodic basis for answering the question about the robustness of predictions for the structure of the QCD phase diagram at the mean-field level discussed here.

We would like to thank O. Kaczmarek for useful comments and discussions. DB acknowledges hospitality and support during his visit at University of Bielefeld and funding of his research provided by the Polish NCN within the “Maestro” grant programme, under contract number UMO-2011/02/A/ST2/00306. GC and AGG acknowledge financial support of CONICET and UNLP (Argentina).

## References

1. M.A. Stephanov, PoS **LAT2006**, 024 (2006).
2. A. Bazavov, T. Bhattacharya, M. Cheng, C. DeTar, H.T. Ding, S. Gottlieb, R. Gupta, P. Hegde *et al.*, Phys. Rev. D **85**, 054503 (2012).
3. N.M. Bratovic, T. Hatsuda, W. Weise, Phys. Lett. B **719**, 131 (2013).
4. S. Carignano, D. Nickel, M. Buballa, Phys. Rev. D **82**, 054009 (2010).
5. M. Kitazawa, T. Koide, T. Kunihiro, Y. Nemoto, Prog. Theor. Phys. **108**, 929 (2002).
6. D. Blaschke, M.K. Volkov, V.L. Yudichev, Eur. Phys. J. A **17**, 103 (2003).
7. T. Hatsuda, M. Tachibana, N. Yamamoto, G. Baym, Phys. Rev. Lett. **97**, 122001 (2006).
8. D. Blaschke, H. Grigorian, A. Khalatyan, D.N. Voskresensky, Nucl. Phys. Proc. Suppl. **141**, 137 (2005).
9. A. Andronic, D. Blaschke, P. Braun-Munzinger, J. Cleymans, K. Fukushima, L.D. McLerran, H. Oeschler, R.D. Pisarski *et al.*, Nucl. Phys. A **837**, 65 (2010).
10. G.A. Contrera, D. Gomez Dumm, N.N. Scoccola, Phys. Lett. B **661**, 113 (2008).
11. G.A. Contrera, M. Orsaria, N.N. Scoccola, Phys. Rev. D **82**, 054026 (2010).
12. D. Horvatic, D. Blaschke, D. Klabucar, O. Kaczmarek, Phys. Rev. D **84**, 016005 (2011).
13. A.E. Radzhabov, D. Blaschke, M. Buballa, M.K. Volkov, Phys. Rev. D **83**, 116004 (2011).
14. S. Benic, D. Blaschke, G.A. Contrera, D. Horvatic, Phys. Rev. D **89**, 016007 (2014).
15. S. Roessner, T. Hell, C. Ratti, W. Weise, Nucl. Phys. A **814**, 118 (2008).
16. A. Dumitru, R.D. Pisarski, D. Zschesche, Phys. Rev. D **72**, 065008 (2005).
17. K. Fukushima, Y. Hidaka, Phys. Rev. D **75**, 036002 (2007).
18. H. Abuki, M. Ciminale, R. Gatto, G. Nardulli, M. Ruggieri, Phys. Rev. D **77**, 074018 (2008).
19. H. Abuki, R. Anglani, R. Gatto, G. Nardulli, M. Ruggieri, Phys. Rev. D **78**, 034034 (2008).
20. D. Gomez Dumm, D.B. Blaschke, A.G. Grunfeld, N.N. Scoccola, Phys. Rev. D **78**, 114021 (2008).
21. V.A. Dexheimer, S. Schramm, Phys. Rev. C **81**, 045201 (2010).
22. B.-J. Schaefer, J.M. Pawłowski, J. Wambach, Phys. Rev. D **76**, 074023 (2007).
23. V. Pagura, D. Gómez Dumm, N.N. Scoccola, Phys. Lett. B **707**, 76 (2012).
24. S. Noguera, N.N. Scoccola, Phys. Rev. D **78**, 114002 (2008).
25. G.A. Contrera, A.G. Grunfeld, D.B. Blaschke, Phys. Part. Nucl. Lett. **11**, 342 (2014).
26. D.B. Blaschke, D. Gomez Dumm, A.G. Grunfeld, T. Klähn, N.N. Scoccola, Phys. Rev. C **75**, 065804 (2007).
27. K. Fukushima, Phys. Rev. D **77**, 114028 (2008).
28. D. Gomez Dumm, N.N. Scoccola, Phys. Rev. C **72**, 014909 (2005).
29. A.V. Friesen, Y.L. Kalinovsky, V.D. Toneev, Int. J. Mod. Phys. A **30**, 1550089 (2015).
30. M.B. Parappilly, P.O. Bowman, U.M. Heller, D.B. Leinweber, A.G. Williams, J.B. Zhang, Phys. Rev. D **73**, 054504 (2006).
31. C.R. Allton, S. Ejiri, S.J. Hands, O. Kaczmarek, F. Karsch, E. Laermann, C. Schmidt, Phys. Rev. D **68**, 014507 (2003).
32. Z. Fodor, S.D. Katz, K.K. Szabo, Phys. Lett. B **568**, 73 (2003).
33. CP-PACS Collaboration (A. Ali Khan *et al.*), Phys. Rev. D **64**, 074510 (2001).
34. O. Kaczmarek, F. Karsch, E. Laermann, C. Miao, S. Mukherjee, P. Petreczky, C. Schmidt, W. Soeldner, W. Unger, Phys. Rev. D **83**, 014504 (2011).
35. R. Bellwied, S. Borsanyi, Z. Fodor, J. Günther, S.D. Katz, C. Ratti, K.K. Szabo, arXiv:1507.07510 [hep-lat].
36. C. Bonati, M. D’Elia, M. Mariti, M. Mesiti, F. Negro, F. Sanfilippo, Phys. Rev. D **92**, 054503 (2015).
37. A. Andronic, P. Braun-Munzinger, J. Stachel, Nucl. Phys. A **772**, 167 (2006).
38. Y.B. Ivanov, Phys. Lett. B **721**, 123 (2013).
39. Y.B. Ivanov, D. Blaschke, Phys. Rev. C **92**, 024916 (2015).
40. C. Sasaki, B. Friman, K. Redlich, Phys. Rev. D **75**, 054026 (2007).
41. S. Borsanyi, Z. Fodor, C. Hoelbling, S.D. Katz, S. Krieg, K.K. Szabo, Phys. Lett. B **730**, 99 (2014).
42. HotQCD Collaboration (A. Bazavov *et al.*), Phys. Rev. D **90**, 094503 (2014).
43. C. Sasaki, K. Redlich, Phys. Rev. D **86**, 014007 (2012).
44. M. Ruggieri, P. Alba, P. Castorina, S. Plumari, C. Ratti, V. Greco, Phys. Rev. D **86**, 054007 (2012).
45. K. Fukushima, K. Kashiwa, Phys. Lett. B **723**, 360 (2013).
46. D.B. Blaschke, F. Sandin, V.V. Skokov, S. Typel, Acta Phys. Pol. Suppl. **3**, 741 (2010).
47. D. Blaschke, M. Buballa, A. Dubinin, G. Roepke, D. Zablocki, Ann. Phys. **348**, 228 (2014).
48. D. Blaschke, A. Dubinin, L. Turko, Phys. Part. Nucl. **46**, 732 (2015).
49. A. Dubinin, D. Blaschke, A. Radzhabov, J. Phys. Conf. Ser. **668**, 012052 (2016).
50. D. Blaschke, A.S. Dubinin, D. Zablocki, PoS **Baldin-ISHEPPXXII**, 083 (2015) arXiv:1502.03084 [nucl-th].